ELSEVIER

Polymer 41 (2000) 3809–3819

polymer

Influence of the loading rate on the fracture resistance of isotactic polypropylene and impact modified isotactic polypropylene

R. Gensler, C.J.G. Plummer*, C. Grein, H.-H. Kausch

Laboratoire de Polymères, Département des Matériaux, École Polytechnique Fédérale de Lausanne, CH-1015 Lausanne, Switzerland

Received 15 July 1999; accepted 17 August 1999

Abstract

The fracture behaviour of an isotactic polypropylene and an impact modified isotactic polypropylene containing 15 wt% of ethylene–propylene rubber has been investigated at test speeds of between 0.1 mm/s and 14 m/s, using compact-tension specimens. The homopolymer displayed a ductile–brittle transition as the test speed was increased, which was associated with a transition from shear deformation to crazing. Deformation of the modified polypropylene was characterized by stable crack propagation over the whole range of test speeds, stress-whitening at the crack tip and, at lower speeds, by the formation of extensive shear lips on the fracture surfaces. An observed increase in the size of the crack tip damage zone with test speed suggested a transition from plane stress to plane strain conditions. This is discussed in terms of a simple model, which takes into account the variation of the sample stress state as the test speed increases.

Keywords: Polypropylene; Impact modified polypropylene; Impact resistance

1. Introduction

There is increasing interest in characterizing the mechanical performance of polymers at high loading rates [1–12]. The primary aim is to provide the designer with reliable data relevant to practical applications, taking into account the fact that the deformation mechanisms and hence the mechanical properties of polymers are often highly rate dependent. Traditional impact tests may prove inadequate in this respect, since they are generally representative of a limited range of effective test speeds and often prove difficult to interpret owing to dynamic effects.

Rate dependent deformation mechanisms are well known to characterize the behaviour of isotactic polypropylene (iPP). In low speed tensile tests at room temperature, unnotched iPP is ductile, provided that its molecular weight is sufficiently high. Under these conditions, typical values for the tensile strain to break are of the order of 500–1000%, depending on the geometry (essentially the thickness) of the samples. However, at higher test speeds and/or at low temperatures iPP usually becomes brittle in tension. Therefore, in order to expand the range of application of iPP, impact modified grades have been developed. The most common modifiers are rubber-like ethylene–propylene copolymers (EPR) and ethylene–propylene–diene monomer elastomers (EPDM) [13,14]. However, in spite of the widespread use of iPP/EPR, iPP/EPDM and related materials (iPP/(polyethylene) PE blends and thermoplastic elastomers based on polyolefins), questions remain concerning their mechanical performance at high loading rates. This is due both to an incomplete understanding of the basic toughening mechanisms in impact modified iPPs, and to the diversity of parameters which may influence their mechanical performance (modifier content, particle size and particle size distribution, modifier morphology, interfaces between the blend components and intrinsic matrix properties).

The aim of the present work has been to study the tensile fracture behaviour of an iPP homopolymer and an iPP/EPR blend with a modifier content of about 15 wt%, over a wide range of test speeds, v, up to and including speeds characteristic of conventional impact tests. The selected molecular weights represent the upper range for widely available commercial materials, and the homopolymer was therefore anticipated to show relatively good fracture toughness under less extreme conditions. The evolution of the fracture toughness with v and the influence of rubber modification will be discussed in the light of the accompanying changes in deformation mechanism.

* Corresponding author.

0032-3861/00/$ - see front matter
PII: S0032-3861(99)00593-5

Table 1
Materials characteristics of the polymers selected for this study; the tensile properties were determined at room temperature and at a crosshead speed of 10 mm/min (the sample thickness was 1 mm)

	iPP homopolymer	iPP/EPR reactor blend
MFI (230°C/2.16 kg)	0.2	0.25
M_w (kg/mol)	455	437
Polydispersity	5.4	5
Modifier content (wt%)	–	15
Tensile modulus (GPa)	1.6	1.25
Tensile yield stress (MPa)	32.5	25
Strain at break (%)	≈880	≈790

2. Experimental

The materials investigated here were provided by PCD Polymere GmbH, Austria, in the form of pellets. Their basic characteristics are summarized in Table 1. The weight average molar mass, M_w, of the homopolymer was 455 kg/mol, and that of the blend was 437 kg/mol.

Plaques with a thickness, B, of approximately 3.8 mm were compression molded at 230°C from the pellets. After melting and compression of the polymers in a first press, the mould was transferred to a second, water-cooled press and rapidly cooled to room temperature. In both materials, the resulting degree of crystallinity of the iPP was about 39 wt% (determined by differential scanning calorimetry at a heating rate of 10 K/min, assuming a heat of fusion $\Delta H_c = 209$ J/g for 100% crystalline iPP [15]).

Notched compact-tension (CT) specimens with dimensions 24×24 mm^2 (width $W = 20$ mm) were machined from the plaques, and a pre-crack introduced by sliding a fresh razor blade over the tip of the notch. The total crack-length, a, was about 10 mm giving $a/W \approx 0.5$. Fracture tests were performed on a servo-hydraulic Schenk high-speed tensile test apparatus, at crosshead speeds, v, of between 0.1 and 14 m/s, and the sample displacement recorded with an optical extensometer [2]. For v greater than 100 mm/s a damping system was employed to minimize perturbations from dynamic effects [2,16,17].

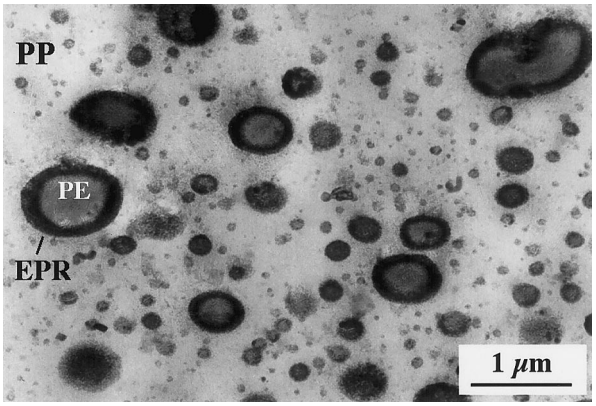

Fig. 1. Microstructure of the iPP/EPR; most of the modifier particles displayed a core-shell structure.

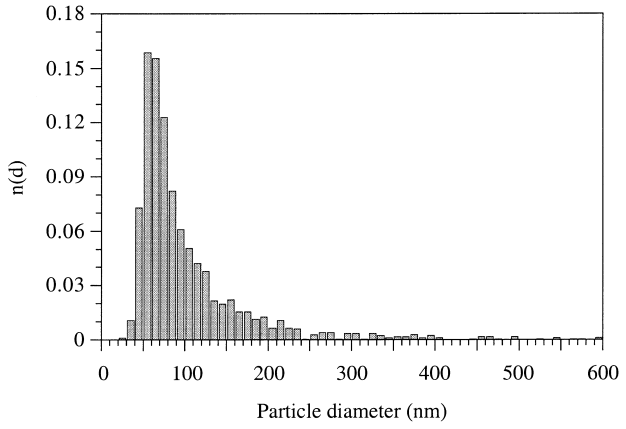

Fig. 2. Particle size distribution of iPP/EPR.

The resistance of the polymer to crack initiation is expressed here in terms of a critical stress intensity factor K_{IQ} [18,19]. K_{IQ} for crack initiation was calculated from the maximum in the load–displacement curves according to the relationship [20]

$$K_{IQ} = f \frac{F_{max}}{BW^{1/2}} \quad (1)$$

where F_{max} is the maximum force in the F–d curve and f is a geometric factor which depends on the ratio a/W. Under conditions of small-scale yielding, that is, where the application of linear elastic fracture mechanics (LEFM) can be justified, K_{IQ} may be considered to be a valid measure of the plane strain critical stress intensity factor, K_{IC}. The extent to which this was true of the present results will be discussed in the next section.

The fracture surfaces of selected CT specimens were examined using a JEOL JSM 6300F Scanning Electron Microscope (SEM) after gold coating. The morphology of the blend and the deformation mechanisms at the crack tips were studied by transmission electron microscopy (TEM). Selected regions were cut from the CT specimens and embedded in an epoxy resin, trimmed and stained in an aqueous solution of RuO_4 for 24 h. Sections of about 150 nm thickness were removed from the stained blocks at room temperature using a Reichert-Jung Ultracut E microtome and a diamond knife, and examined using the Philips CM 20 (acceleration voltage 200 kV). The mean particle size and the particle size distribution in sections from undeformed samples of the blend were estimated from TEM micrographs using the Graftek OptiLab-Pro image analysis software package.

3. Results and discussion

3.1. Sample morphology

All the specimens displayed a fully spherulitic microstructure containing essentially α phase lamellae (β

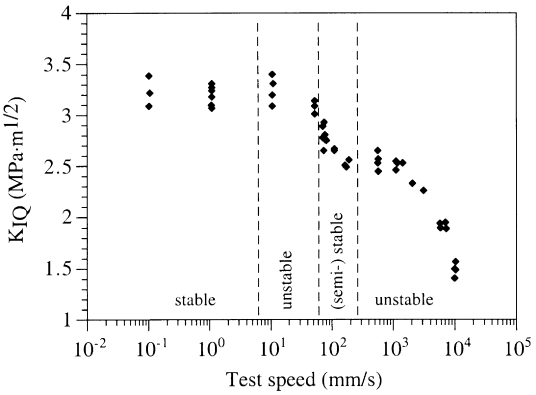

Fig. 3. Variation of the stress intensity factor K_{IQ} of iPP as a function of v; mode of crack propagation as indicated.

spherulites were observed only sporadically). Fig. 1 shows a TEM micrograph of the local microstructure of the blend. Most of the modifier particles showed a core-shell structure, with a lamellar PE rich core and an amorphous EPR shell (for convenience we shall henceforth refer to the modifier phase as EPR). Some of the larger particles nevertheless contained several PE inclusions. The average diameter of the EPR domains in the sections was 110 nm and the corresponding distribution was highly asymmetric (Fig. 2). The mean particle diameter in the bulk must be assumed to be somewhat different from the above value since in many cases the TEM images correspond neither to projections of the whole particles nor to equatorial sections (particularly in the case of the largest particles).

3.2. Fracture properties of iPP as a function of v

The variation of K_{IQ} with v for the homopolymer is shown in Fig. 3, and typical $F–d$ curves are shown for different v in Fig. 4. For $v < 10$ mm/s, K_{IQ} was of the order of 3.2 MPa $m^{1/2}$, and crack propagation was stable. Between 10 and 70 mm/s fracture became more brittle. At 10 mm/s the $F–d$ curves still displayed some non-linearity before the load reached its maximum value, but this was substantially suppressed as v increased further. At the same time, K_{IQ} decreased from 3.2 MPa $\cdot$ $m^{1/2}$ to about 1.5 MPa $\cdot$ $m^{1/2}$ (see Fig. 3). An intermediate regime of stable or semi-stable crack propagation was observed between 70 and 200 mm/s, as indicated by Fig. 4, but fully brittle behaviour returned at higher v. The $F–d$ curves were almost linear for $v \geq 2$ m/s.

The occurrence of two stable–unstable transitions as v is increased is thought to be due to two competing effects: (a) with increasing v the time required for the relaxation of

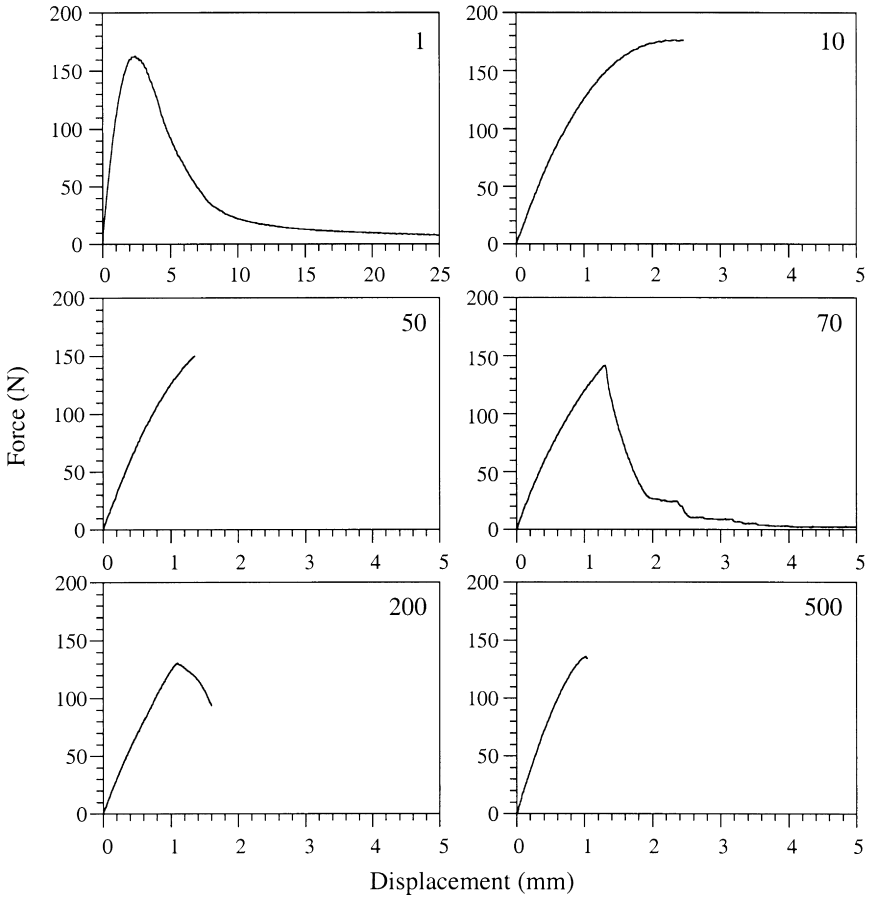

Fig. 4. Force–displacement curves of iPP at different v (v is given in mm/s).

Table 2
Validity of the calculated stress intensity factors; the yield stress (σ_y) data were taken from Van der Wal [21] (for the definition of A see Eq. 2)

	Test speed		
	≈10 mm/s	≈1 m/s	≈5 m/s
Mode of crack propagation	Unstable	Unstable	Unstable
K_{IQ} (MPa · m$^{1/2}$)	3.2	2.5	2
σ_y (MPa)	42	53	60
A (mm)	14.5	5.5	2.8

stress concentrations at the crack tip becomes comparable with, and eventually exceeds the effective time available, which is determined by v; (b) at high v, energy dissipated in the form of heat is no longer conducted away from the crack tip in times comparable with that of the test, and the temperature at the crack tip increases, resulting in local softening of the material (some authors suggest that the temperature rise may be sufficient to induce local melting of the polymer in the vicinity of the crack trajectory [11,21,22]). The first stable–unstable transition at about 10 mm/s may be attributed to effect (a), since the influence of adiabatic heating is not thought to be significant at this test speed. However, adiabatic heating has been shown to become important at higher v. Van der Wal [21], for example, has used an infrared camera to measure a temperature rise of about 50 K at the crack tip in EPDM modified iPP samples deformed at 1 m/s. The onset of stable crack propagation in the iPP samples at $v \approx 100$ mm/s was therefore attributed to adiabatic heating and the associated local softening of the material in the vicinity of the crack tip (effect (b)). As v was increased further, however, effect (a) presumably became dominant again.

The K_{IQ} for the lowest v corresponded well with the literature values for the plane strain critical stress intensity, K_{IC} (the low speed K_{IC} of high molecular weight iPP is typically between 3 and 4 MPa · m$^{1/2}$ [23,24]). Nevertheless, strictly valid K_{IC} determination requires linear-elastic behaviour up to the point of fracture, and for the homopolymer this was only the case at very high v. According to LEFM-based

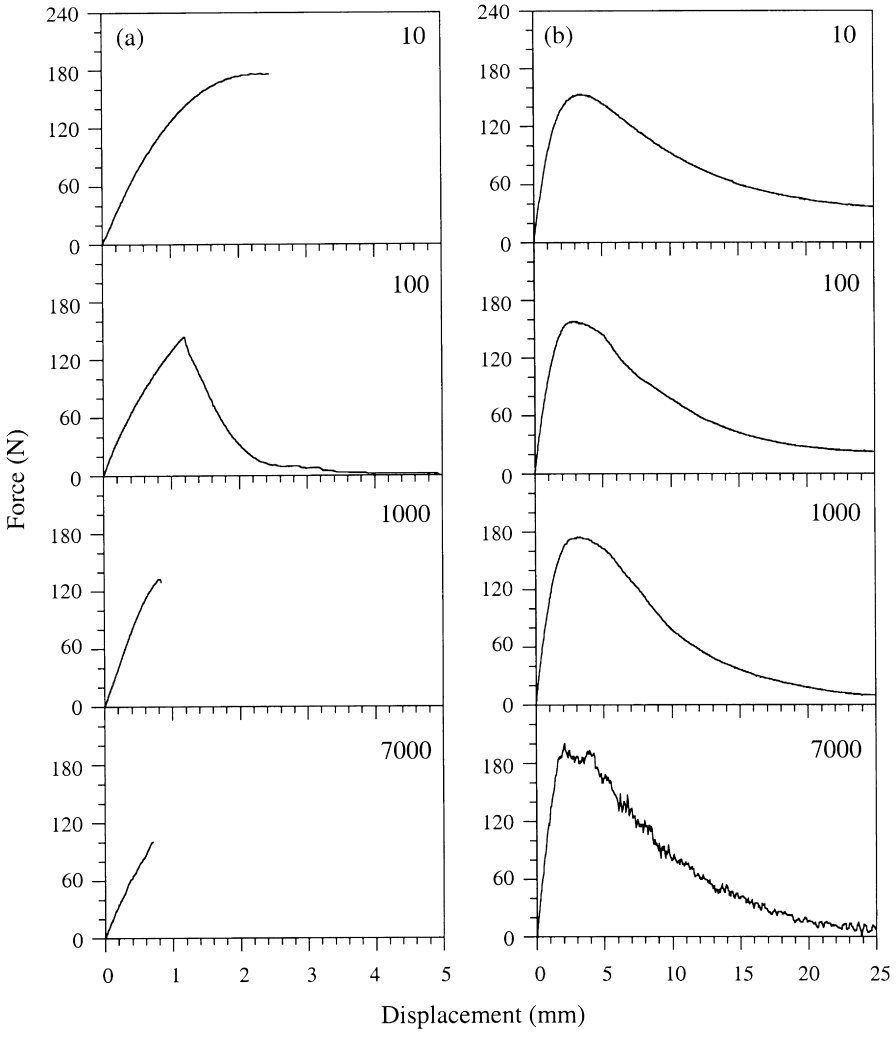

Fig. 5. Comparison of typical force–displacement curves of (a) iPP and (b) iPP/EPR at different v (indicated in mm/s; note also the different graduation of the x-axis).

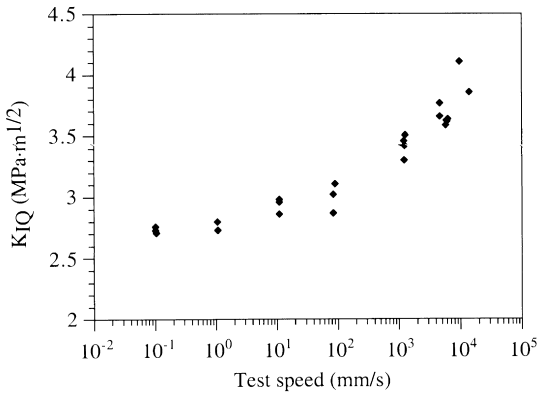

Fig. 6. Variation of the stress intensity factor K_{IQ} of the iPP/EPR blend.

standard test protocols a stress intensity factor K_{IQ} may be considered to correspond to the critical plane strain stress intensity factor K_{IC} if the following conditions are fulfilled [20]:

$$(W - a), B, a \geq 2.5\left(\frac{K_{IQ}}{\sigma_y}\right)^2 = A \tag{2}$$

For the CT specimens used here, the quantities $(W - a)$, a and B were about 10, 10 and 3.8 mm, respectively, and values for the yield stress, σ_y, have been given by Van der Wal [21] as a function of v. Table 2 summarizes the results of the calculations for three different v at which the samples failed by unstable crack propagation. The stress

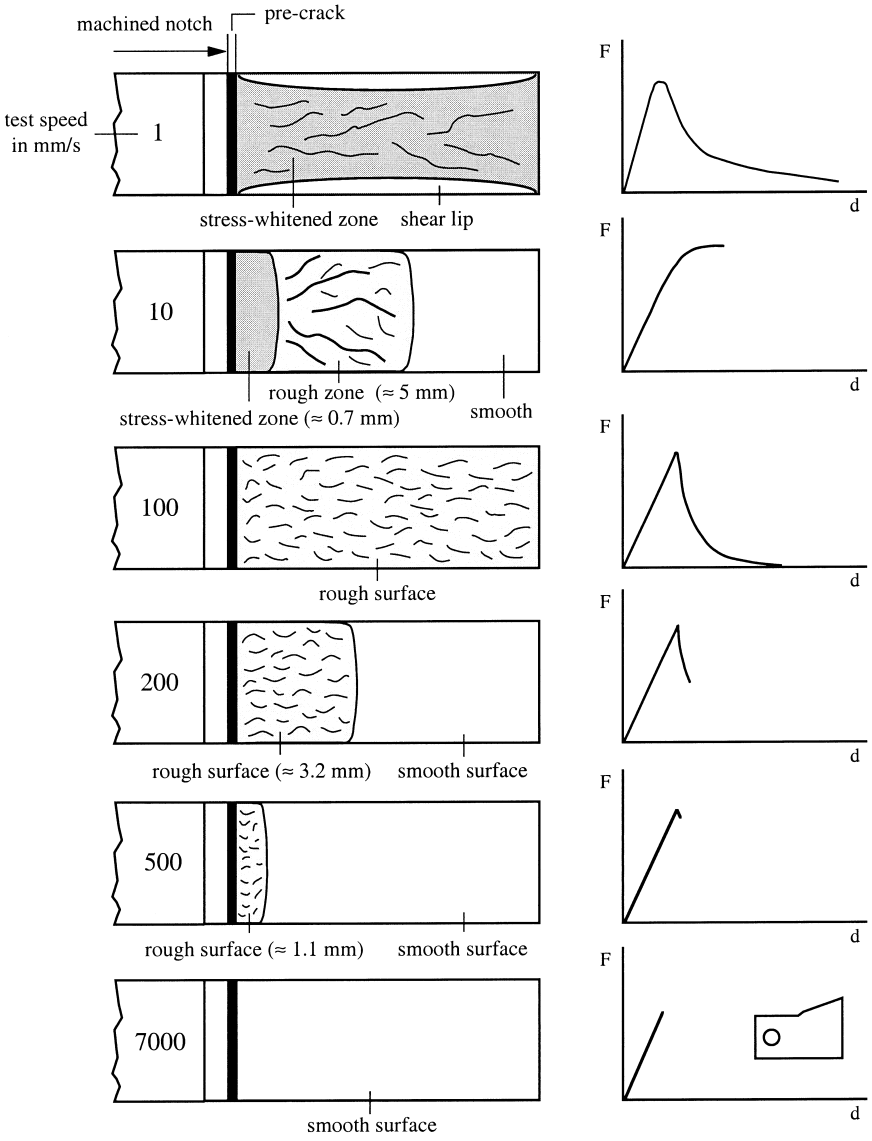

Fig. 7. Schematic representation of the fracture surfaces of iPP CT specimens as a function of v along with the corresponding F–d curves; at very high speeds the crack deviates from the horizontal.

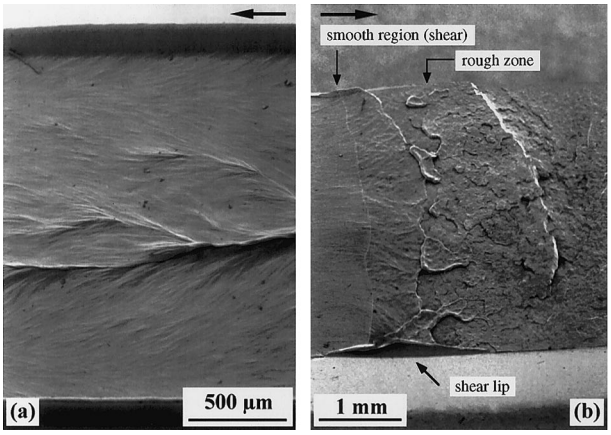

Fig. 8. SEM micrographs of fracture surfaces of iPP specimens deformed at (a) 1 mm/s and (b) 10 mm/s; the crack propagation direction is indicated by the arrows.

intensity factors listed represent typical experimental values (see Fig. 3).

At 10 mm/s the conditions of Eq. 2 were not fulfilled, and the deformation behaviour must be assumed to have been strongly influenced by plane stress conditions (a sample thickness of about 14.5 mm would have been necessary to ensure plane strain conditions). At 1 m/s, however, plane strain conditions were close to being met, the theoretically required sample thickness of 5.5 mm being only slightly higher than the actual thickness of the CT specimens (it is also likely that the yield stresses given in Table 2 are conservative estimates, given the localized nature of yielding in notched CT specimens). Finally, for $v = 5$ m/s the criteria given by Eq. 2 were entirely satisfied, and the measured stress intensity factors therefore represent valid K_{IC}.

3.3. Fracture properties of iPP/EPR as a function of v

Typical $F–d$ curves for the blend are shown in Fig. 5 along with $F–d$ plots for the homopolymer obtained at comparable v. Whereas the homopolymer showed multiple transitions, as discussed previously, stable crack propagation was observed in the blend over the entire range of v.

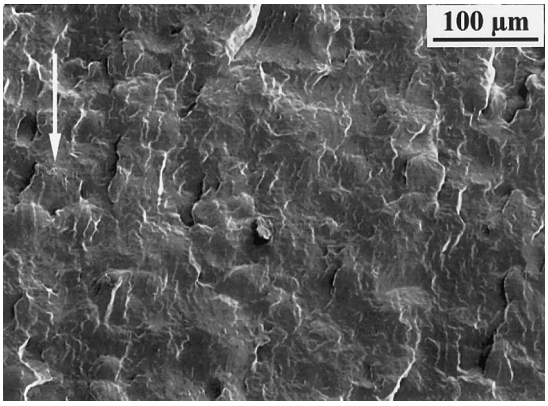

Fig. 9. Fracture surface of an iPP specimen deformed at about 10 m/s.

Moreover, the force maximum in the $F–d$ curves was found to increase with increasing v, reflecting the rate dependence of the yield stress of the material. At high rates ($v \geq 3$ m/s) dynamic effects were present, but the force and the displacement signals remained exploitable at v of up to 14 m/s.

The variation of K_{IQ} with v is shown in Fig. 6. Below $v \approx 50$ mm/s the K_{IQ} of the iPP/EPR blend was less than that of the homopolymer, reflecting the lower yield stress of the material. However, the fracture resistance of the blend was significantly improved at high speeds, that is, under impact conditions. Although the K_{IQ} values for the blend did not represent valid plane strain fracture toughness data according to the criteria introduced in the previous section, they remain useful, since K_{IQ} continues to reflect a critical stress state for crack initiation. For comparison, typical low speed plane strain fracture toughness values for EPR and PE modified iPP are of the order of $3\ \mathrm{MPa \cdot m^{1/2}}$ [25–28], depending on the test temperature and the blend composition.

3.4. Deformation mechanisms in iPP

The appearance of the fracture surfaces of the iPP specimens is sketched in Fig. 7 for different v, along with the corresponding $F–d$ curves. During stable crack propagation at the lowest speeds (0.1–1 mm/s), the occurrence of pronounced shear lips reflected the predominantly plane stress conditions. The fracture surfaces were highly stress-whitened and relatively smooth, as can be seen in the SEM micrograph in Fig. 8(a).

Although crack propagation became unstable at 10 mm/s, the $F–d$ curves continued to show pronounced non-linearity prior to fracture. The fracture surfaces showed three distinct zones in this case. A highly stress-whitened, smooth region of about 0.7 mm in length and associated with shear deformation as previously, was observed close to the pre-crack (Fig. 8(b); small shear lips are also visible in this micrograph). Beyond the smooth region, there was a rough but unwhitened zone of about 5 mm in length. The remainder of the fracture surface was again smooth, in this case reflecting unstable crack propagation.

In the range 70–100 mm/s, corresponding to the transition back to stable crack propagation, the fracture surfaces were relatively rough, un-whitened and uniform in appearance over their entire length. Stable–unstable crack propagation at higher v resulted in similar fracture surfaces, with the exception of a smooth region due to unstable crack propagation in the later stages of the test. The relative extent of the smooth region increased with further increases in v, constituting the entire fracture surface at 1 m/s and above (Fig. 9). Finally, for $v \geq 5$ m/s the cracks began to deviate from their ideal horizontal trajectory owing to the increasing influence of mode II loading [16].

The onset of brittle failure and the appearance of a rough zone on the fracture surfaces were associated with multiple craze formation (giving rise to dark streaks in TEM

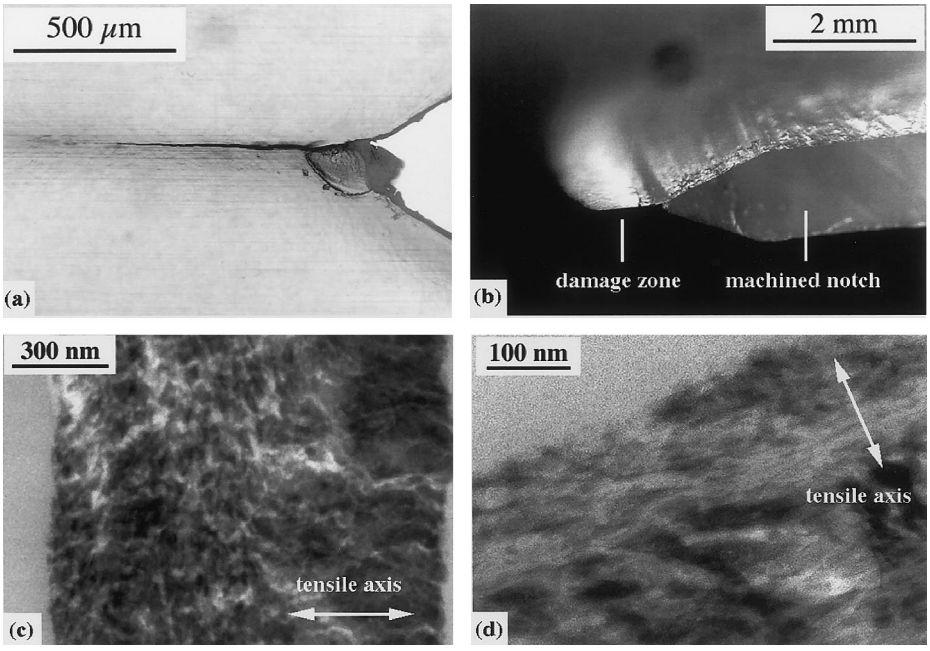

Fig. 10. (a) Side-view of the crack-tip damage zone of an iPP CT sample deformed at about 3 m/s; (b) oblique of the damage zone showing the curved deformation front; (c) TEM micrograph of the collapsed fibrillar structure of the crack-tip craze; (d) detail of structure at the craze–bulk interface.

micrographs of thin sections from the damage zone in stained samples). The surface roughness itself was thought to be due to the superposition of multiple cracks, initiating within the crazes at different times and in slightly different planes. The decrease in size of the rough zone with increasing v was therefore taken to imply a decrease in the extent of multiple crazing. Thus, at very high loading rates, for which the fracture surfaces were smooth, it was assumed that crack propagation proceeded via the formation of a single crack-tip craze (a transition from multiple crazing to single craze extension with increasing test speed was also observed for polycarbonate [16] and rubber toughened poly(methyl methacrylate) [2]). To verify this we carried out additional fracture tests using the "twins method", in which two CT samples are tested in series [16]. Since the pre-crack length is slightly different for the two specimens, fracture of one specimen leads to rapid unloading of its twin. Although the second specimen does not fail, it experiences a peak load, which is in general sufficient to initiate deformation at the crack tip. As is clear from Fig. 10(a), a single localized damage zone was indeed present at the crack tip of iPP CT samples tested at high speeds (the crosshead speed for the specimen shown in Fig. 10(a) was 3 m/s). In Fig. 10(b), the plane of the damage zone is inclined with respect to that of the image, revealing slight curvature of its front. The TEM analysis of thin sections taken from the damage zone revealed the presence of a collapsed fibrillar structure which is typical of that of an unloaded craze (Fig. 10(c)). Fig. 10(d) shows a detail of the craze. Close inspection of this image suggests a periodicity of about 10–20 nm, which is assumed to reflect that of the original craze fibrils (as a result of RuO_4 staining the darker regions correspond to voids). The deformation mechanisms in the damage zone at the crack tip are summarized in Fig. 11 as a function of v.

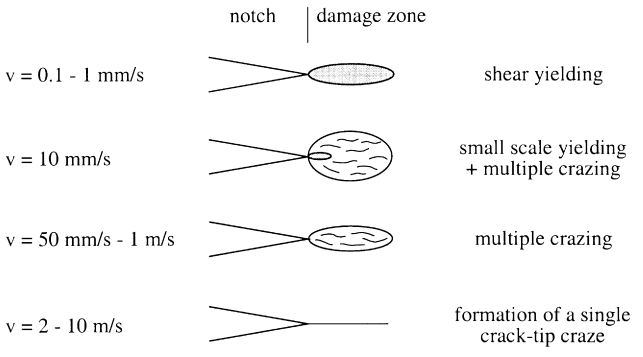

Fig. 11. Deformation mechanisms in the damage zone of iPP CT samples as a function of v.

The existence of a single crack-tip craze at high test speeds justifies comparison of K_{IC} with estimates in terms of molecular parameters, obtained using the model of Brown [29]:

$$K_{IC} = \Sigma f_s \left(\frac{2\pi E D_0}{(1-\mu^2) S_c} \right)^{1/2} \alpha^{1/4} \left(1 - \frac{1}{\lambda} \right)^{1/2} \quad (3)$$

where $\Sigma \approx 3.2 \times 10^{17}/m^2$ is the areal density of entangled chains in the craze fibrils (assuming the entanglement density $v_e = 16 \times 10^{25}/m^3$ [30]), $f_s \approx 2$ nN is the force to break or to disentangle a chain [24], $D_0 \approx 10$ nm is the mean fibril diameter [31], S_c is the stress perpendicular to the craze surface, α (is a factor which describes the elastic anisotropy of the craze fibrils, E is the bulk tensile modulus,

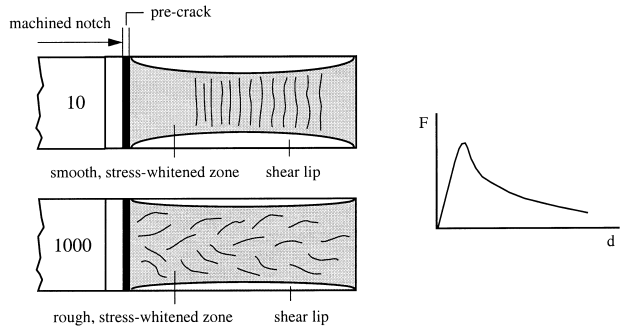

Fig. 12. Sketch of the fracture surfaces of iPP/EPR specimens deformed at about 10 and 1000 mm/s.

μ is Poisson's ratio and $\lambda \approx 4.5$ [30] is the fibril draw ratio. Eq. 3 has already been successfully applied to reaction bonded interfaces between iPP and Polyamide 6 in which a single craze has been shown to propagate along the iPP side of the interface prior to fracture, although certain of the quantities listed above are difficult to estimate [31].

Under the present conditions, that is for $v > 2$ m/s, μ and E were taken to be 0.35 [32] and 2 GPa, respectively (indeed, at 10 mm/min, the tensile modulus is already 1.6 GPa, as indicated in Table 1). S_c, was equated with the bulk yield stress at high strain rates (a value of $\sigma_y = 60$ MPa has been obtained by Van der Wal for v of about 5 m/s [21]). Finally, the value of α(is unknown for iPP, and that for PMMA ($\alpha \approx 40$ [29]) was used here. The plane strain stress intensity factor obtained from Eq. 3 using these data was $K_{IC} = 2.19\ \text{MPa} \cdot \text{m}^{1/2}$. This value falls well within the range of the measured stress intensity factors for $v \geq 2$ m/s in which regime plane strain conditions have been shown to apply.

3.5. Deformation mechanisms in iPP/EPR

All the iPP/EPR CT specimens failed by stable crack propagation. This suggests that the deformation of the

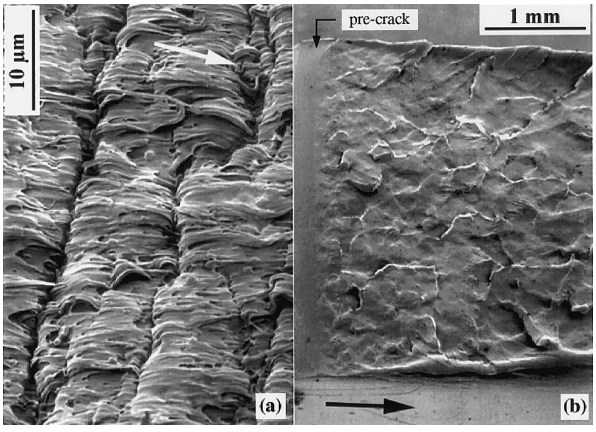

Fig. 13. SEM of the fracture surfaces of iPP/EPR samples deformed at (a) 10 mm/s and (b) 5.8 m/s; the crack-propagation direction is indicated by the arrows.

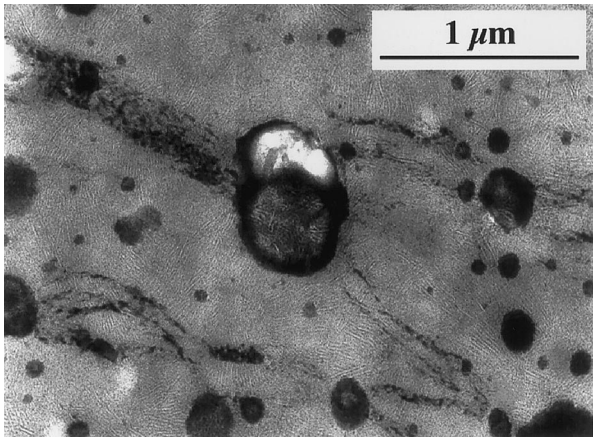

Fig. 14. TEM micrograph showing crazing and rubber particle breakdown in an iPP/EPR sample close to the fracture surface; the sample was deformed at about 7 m/s.

samples was primarily governed by shear processes in the iPP matrix. At low and intermediate speeds ($v \leq 100$ mm/s) pronounced shear lips were observed in the iPP/EPR samples, as sketched in Fig. 12, and the fracture surfaces were generally smooth and highly stress-whitened. At a certain distance from the pre-crack, characteristic striations oriented parallel to the sample thickness were observed. A SEM micrograph of these structures is shown in Fig. 13(a). They are thought to have originated from a step-wise release of stored energy in the specimen during crack propagation. Voids due to the breakdown of rubber particles were also occasionally seen on the fracture surfaces. However, close inspection of the SEM micrographs suggested that only the large modifier particles were associated with void formation.

When v was increased to 1000 mm/s, the striations were

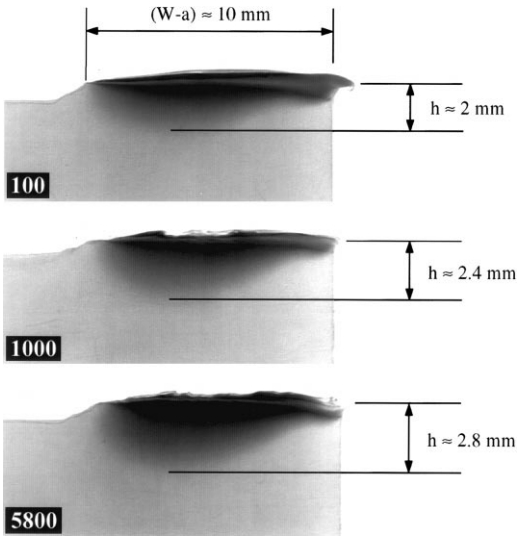

Fig. 15. Side-view of fractured iPP/EPR CT specimens (in reverse contrast); the height, h, of the stress-whitened zone parallel to the loading direction increases with increasing v (given here in mm/s); note also the decrease of the size of the shear lips with increasing speed.

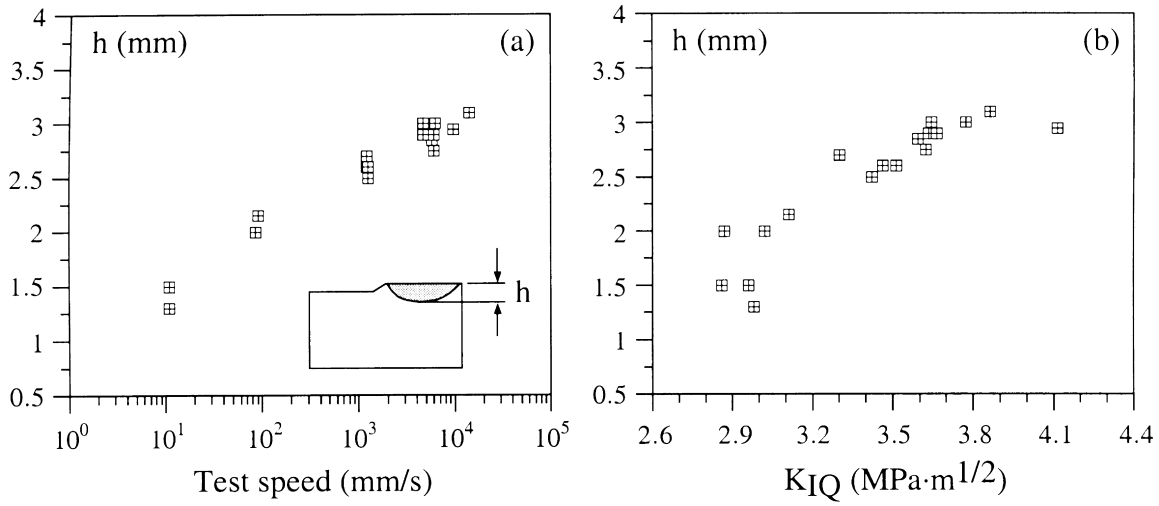

Fig. 16. Width, *h*, of the stress-whitened zone in iPP/EPR samples as a function of (a) *v* and (b) the stress intensity factor K_{IQ}.

no longer visible on the fracture surfaces (Fig. 12). The fracture surfaces were again stress-whitened but unlike at lower testing speeds, were relatively rough. The size of the shear lips also decreased significantly, suggesting a gradual change from plane stress to plane strain behaviour and the suppression of shear processes. Fig. 13(b) shows the region close to the pre-crack of a specimen tested at about 5.8 m/s. The appearance of the fracture surface suggests failure to have involved the propagation of several cracks. Since the stress state was thought to change gradually from plane stress to plane strain with increasing *v*, crazing in the iPP matrix may be expected to become important for $v \geq 1$ m/s (high deformation speeds generally favor cavitational processes). The deformation mechanisms in the damage zone of samples deformed at about 7 m/s were therefore investigated in more detail by TEM. As shown in Fig. 14, craze-like structures were indeed present in the vicinity of the fracture surface, generally initiating at the EPR particles, although they were absent at low *v*. Cavitation of the large central rubber particle is also apparent in Fig. 14.

Side-views of fractured iPP/EPR specimens deformed at three different test speeds are shown in Fig. 15 (for better reproduction the images are shown in reverse contrast). The width, *h*, of the plastic zone parallel to the loading direction was found to increase with increasing *v*. The gray level in the stress-whitened zone decreased with increasing distance from the fracture plane. This is a direct indication of the presence of a deformation gradient at the crack tip resulting from the decreasing stress intensity with increasing distance from the fracture plane. For quantitative analysis of this

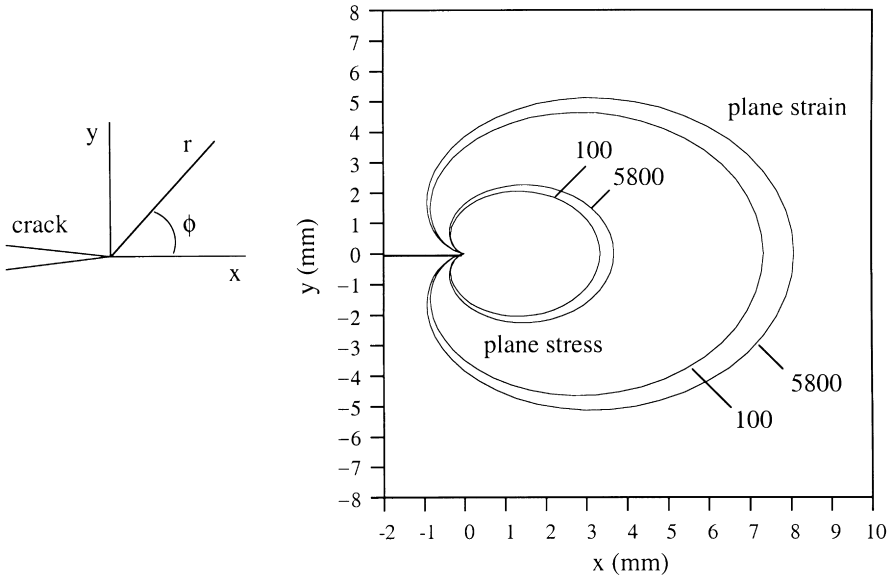

Fig. 17. Calculated shape of the plastic zone ahead of the crack tip in CT specimens of the iPP/EPR blend as a function of *v* (100 and 5800 mm/s) and stress state.

phenomenon the height, h, of the stress-whitened zone was measured using a travelling microscope. The h values are plotted in Fig. 16(a) as a function of v and in Fig. 16(b) as a function of K_{IQ}. h increased almost linearly with the logarithm of v and from Figure 16(b) it is clear that the dimensions of the stress-whitened zone were influenced by the stress concentration at the crack tip.

To account for the plastic zone size and shape in rubber toughened polycarbonate, Kayano et al. [33] have assumed that the size of the damage zone is dependent on the sample volume in which cavitation processes are activated in the modifier domains. Cavitation of the rubber particles accompanied by intense stress whitening was also observed in the iPP/EPR blend studied here (see Fig. 14), providing some justification for the use of this model.

According to LEFM, the stress state in the vicinity of a sharp crack in mode I opening is characterized by the stress intensity factor K_I. The principal stresses at a distance r from the crack tip and at an angle ϕ(to the direction of crack propagation are given by the following equations [18,19] (for the definition of r and ϕ(see Fig. 17):

$$\begin{pmatrix}\sigma_1\\ \sigma_2\end{pmatrix} = \frac{K_I}{\sqrt{2\pi r}}\begin{pmatrix}\cos\frac{\phi}{2}\left(1+\sin\frac{\phi}{2}\right)\\ \cos\frac{\phi}{2}\left(1-\sin\frac{\phi}{2}\right)\end{pmatrix} \tag{4}$$

For plane strain

$$\sigma_3 = \frac{K_I}{\sqrt{2\pi r}} 2\mu \cos\frac{\phi}{2}$$

For plane stress

$$\sigma_3 = 0$$

Strain components can be expressed in terms of the principal stresses [34],

$$\begin{pmatrix}\varepsilon_1\\ \varepsilon_2\\ \varepsilon_3\end{pmatrix} = \begin{pmatrix}\frac{1}{E}[\sigma_1 - \mu(\sigma_2+\sigma_3)]\\ \frac{1}{E}[\sigma_2 - \mu(\sigma_1+\sigma_3)]\\ \frac{1}{E}[\sigma_3 - \mu(\sigma_1+\sigma_2)]\end{pmatrix} \tag{5}$$

Cavitation is assumed to occur when the volume strain, ε_v, exceeds a critical value, ε_{vc}.

$$\varepsilon_v = (1+\varepsilon_1)(1+\varepsilon_2)(1+\varepsilon_3) - 1 > \varepsilon_{vc} \tag{6}$$

The size and the shape of the plastic zone, $r(\phi)$, at the crack tip can then be determined from Eq. 6. The plastic zones shown in Fig. 17 were calculated using $\mu = 0.43$ [35] and the following parameters: (a) $v = 100$ mm/s, $E = 1.4$ GPa [35], $K_{IQ} = 3$ MPa $\cdot$ m$^{1/2}$; (b) $v = 5800$ mm/s, $E = 1.6$ GPa [35], $K_{IQ} = 3.6$ MPa $\cdot$ m$^{1/2}$ (see Fig. 6). The critical volume strain, ε_{v0}, required for cavitation of EPR particles was not known, and it was therefore assumed that $\varepsilon_{v0} = 0.4\%$ a value suggested by Bucknall [36] to be appropriate to natural rubber.

The shape of the calculated cavitation zone corresponded reasonably well to the observed shape of the stress-whitened zone. For plane strain conditions, the calculations predicted a significantly larger plastic zone than for plane stress conditions (this contrasts with what would be expected for the von Mises criterion, according to which the size of the plastic zone under plane strain conditions should be smaller than under plane stress conditions [18,19]). On this basis, the toughening effect of rubber particles under plane stress conditions would be expected to be less significant than under plane strain conditions. Moreover, the contribution of cavitation processes (either in the form of rubber particle voiding or crazing) to the total volume strain would be expected to decrease with decreasing v, if the decrease in v is sufficient to provoke a transition from plane strain to plane stress. This has been observed experimentally in a variety of rubber toughened materials, including rubber modified iPP [2,35].

Under both plane stress and plane strain conditions, the calculated size of the plastic zone increased with increasing v. At a speed of 100 mm/s and under plane stress conditions, the calculated maximum extent of the cavitation zone in the loading direction (y) was about 2 mm, in reasonable agreement with observed zone sizes in the iPP/EPR specimens tested at 100 mm/s (Fig. 16(a)). The occurrence of shear lips as well as the general appearance of the fracture surfaces of these specimens were also suggestive of plane stress conditions. On the other hand, if deformation of the samples tested at 5800 mm/s is assumed to have occurred under fully plane strain conditions, then according to the model, the size of the cavitation zone would have been significantly larger than the observed dimensions of the stress-whitened zone. However, the continued presence of small shear lips at high v suggested the transition to plane stress conditions to be incomplete. The extent of the cavitation zone parallel to y was therefore to be expected to be in the range $h =$ 2.2–5 mm (see Fig. 17). The measured value of h was 3 mm at 5800 mm/s.

4. Conclusions

The fracture behaviour of a high molecular weight iPP homopolymer and an iPP/15 wt% EPR reactor blend has been investigated as a function of v. The main results were as follows:

(i) The iPP homopolymer displayed a ductile–brittle transition with increasing v. The loss in ductility was due to changes in the deformation mechanisms. Highly dissipative shear processes dominated at low speeds ($v \leq 1$ mm/s), and multiple crazing at intermediate speeds ($v = 50$–1000 mm/s). At $v \geq 2$ m/s, crack tip damage was limited to a single localized deformation zone (single crack-tip craze). The changes of the

deformation mechanisms with increasing *v* were not only reflected by the evolution of the appearance of the fracture surfaces but also by the shape of the load-displacement curves.

(ii) The fracture resistance of the iPP/EPR blend was superior to that of the homopolymer. No ductile–brittle transition was observed in the range of *v* considered here, and most of the deformation energy was absorbed by shear processes in the iPP matrix. Coarse craze-like structures were observed at elevated *v* close to the fracture surface but appeared to be suppressed at low speeds.

(iii) The extent of the stress-whitened zone at the crack tip in iPP/EPR was found to increase with increasing *v*. This suggests that under impact conditions, deformation processes were activated in a significantly larger sample volume. Model calculations were carried out in order to account for the influence of *v* and the stress state on the size of the stress-whitened zone parallel to the loading direction, giving results in reasonable agreement with the experimental observations.

Acknowledgements

The electron microscopy work was carried out in the Electron Microscopy Center (CIME) of the École Polytechnique Fédérale de Lausanne, and we are indebted to Brian Senior (CIME) for his assistance with the SEM analysis. Thanks are also due to Djahandar Tafazzoli for his help with the fracture tests, and to Dr Philippe Béguelin (Laboratoire de Polymères, École Polytechnique Fédérale de Lausanne) for helpful discussions. R.G. gratefully acknowledges the support of the Ciba Speciality Chemicals Inc., Switzerland.

References

[1] Williams JG, Pavan A, editors. Impact and dynamic fracture of polymers and composites London: Mechanical Engineering Publications, 1995.
[2] Béguelin P, PhD thesis 1572, Ecole Polytechnique Fédérale de Lausanne, 1996.
[3] Béguelin P, Kausch HH. J Mater Sci 1994;29:91.
[4] Béguelin P, Kausch HH. J Phys IV France 1997;7:933.
[5] Plummer CJG, Béguelin P, Kausch HH. Polym Engng Sci 1995;35:1300.
[6] Lu ML, Chiou KC, Chang FC. Polym Engng Sci 1996;36:2289.
[7] Julien O, Béguelin P, Monnerie L, Kausch HH. In: Riew CK, Kinloch AJ, editors. Toughened plastics II, Washington, DC: American Chemical Society, 1996. p. 233.
[8] Hamdan S, Swallowe GM. J Mater Sci 1996;31:1415.
[9] Hashemi S. Polym Eng Sci 1997;37:912.
[10] Gensler R, Béguelin P, Plummer CJG, Kausch HH, Münstedt H. Polym Bull 1996;37:111.
[11] Steenbrink AC, Janik H, Gaymans RJ. J Mater Sci 1997;32:5505.
[12] Chou CJ, Vijayan K, Kirby D, Hiltner A, Baer E. J Mater Sci 1988;23:2521–33.
[13] Utracki LA, Dumoulin MM. Ch. 3. In: Karger-Kocsis J, editor. Polypropylene: structure, blends and composites, 2. London: Chapman & Hall, 1995.
[14] Dwyer SM, Boutni OM, Shu C. Ch. 5. In: Moore EP, editor. Polypropylene handbook, Munich: Hanser, 1996.
[15] Quirk RP, Alsamarraie MAA. In: Brandrup J, Immergut EH, editors. Polymer handbook, New York: Wiley, 1990. p. V27.
[16] Béguelin P, Kausch HH. In: Williams JG, Pavan A, editors. Impact and dynamic fracture of polymers and composites, London: Mechanical Engineering Publications, 1995. p. 3.
[17] Béguelin P, Barbezat M, Kausch HH. J Phys III France 1991;1:1867.
[18] Williams JG. Fracture mechanics of polymers, Chichester: Ellis Horwood, 1984.
[19] Anderson TL. Fracture mechanics - fundamentals and applications, Boca Raton, FL: CRC Press, 1995.
[20] Williams JG, Cawood MJ. Polym Testing 1990;9:15.
[21] Van der Wal A, PhD thesis, University of Twente, 1996.
[22] Dijkstra K, PhD thesis, University of Twente, 1993.
[23] Mai YW, Williams JG. J Mater Sci 1977;12:1376.
[24] Kausch HH. Polymer fracture, Berlin: Springer, 1987.
[25] Fernando PJ, Williams JG. Polym Engng Sci 1980;20:215.
[26] Fernando PL, Williams JG. Polym Engng Sci 1981;21:1003.
[27] Hodgkinson JM, Savadori A, Williams JG. J Mater Sci 1983;18:2319.
[28] Hornsby PR, Premphet K. J Mater Sci 1997;32:4767.
[29] Brown HR. Macromolecules 1991;24:2752.
[30] Plummer CJG, Kausch HH. Macromol Chem.Phys 1996;197:2047.
[31] Plummer CJG, Kausch HH, Creton C, Kalb F, Léger L. Macromolecules 1998;31:6164.
[32] Schreier G. Konstruieren mit kunststoffen, Munich: Hanser, 1972.
[33] Kayano Y, Keskkula H, Paul DR. Polymer 1998;39:821.
[34] Ward IM, Hadley DW. An introduction to the mechanical properties of solid polymers, Chichester: Wiley, 1993.
[35] Grein C, Ecole Polytechnique Fédérale de Lausanne, unpublished results, 1998.
[36] Bucknall CB, Karpodinis A, Zhang XC. J Mater Sci 1994;29:3377.